PCCP

PAPER

View Article Online
View Journal | View Issue

Cite this: *Phys. Chem. Chem. Phys.*, 2017, **19**, 28458

Towards a taxonomy of topology for polynuclear aromatic hydrocarbons: linking electronic and molecular structure†

Erin M. Adkins and J. Houston Miller*

Received 4th September 2017,
Accepted 10th October 2017

DOI: 10.1039/c7cp06048c

rsc.li/pccp

Trends linking the topological characteristics of polynuclear aromatic hydrocarbons (PAH) to their electronic properties are reported. TD-DFT electronic spectra computations, using the 6-31G* basis set and B3LYP exchange correlation functional, were calculated for a series of PAH, allowing for the HOMO–LUMO gaps to be reported. Clar structures provide an avenue to link the physical structure and the aromaticity of the molecule; which, when extended by bond length and harmonic oscillator model of aromaticity analysis, provide powerful tools to understand the link between electronic and physical structure. These results lead to the conclusion that all PAH structures show a decrease in HOMO–LUMO gap as a function of size, but the rate of that decrease is directly related to the topology of the molecules. A PAH taxonomy was developed that categorizes PAH into categories with similar topological properties, which allows for modelling of changes in the HOMO–LUMO gap with PAH size. An atom-pair minimization algorithm was used to calculate the binding energy (BE) of homogeneous dimers of the studied PAH. The BE per carbon atom increases with the overall size of the structure to an asymptotic limit, but as with the HOMO–LUMO gap, topology plays a critical secondary factor. Previously published, experimentally determined optical band gaps (OBG) from Tauc/Davis–Mott analysis of extinction spectra in various laminar, non-premixed flames produced a correlation between the HOMO–LUMO gaps of high-symmetry, nearly circular D_{2h} symmetry molecules to molecular size. The work presented here provides a much more nuanced and predictive evaluation of how OBG depends on structure and size.

Introduction

Polynuclear aromatic hydrocarbons (PAH), compounds composed of fused aromatic rings,[1] are often the most thermodyamically stable isomeric form for given inventories of carbon and hydrogen atoms.[2] Thus, these ubiquitous molecules have been the focus of inquiry across several areas of science including the literature of asphaltenes, interstellar dust and gas clouds, combustion research, and, most recently, studies of graphene.[3–7] Similar structural features also appear in fullerenes and nanotubes, and, because these classes of materials share similar bonding, similar diagnostic tools have been applied to their study.

Our lab's interest in PAH has centred on their role as intermediates in the formation of carbonaceous, nanoscale, particulate matter (*i.e.*, soot) in combustion systems. The results of this work has appeared in several manuscripts over the past decade and is summarized below.[8–16] It is generally held that particle formation in flames begins with cyclization reactions of unsaturated hydrocarbon radicals to form benzene.[17–24] Subsequent growth occurs through hydrogen abstraction followed by successive acetylene addition (known as the HACA mechanism)[19] leading to larger PAH. Incipient particulate coalesce from these larger PAH into roughly spherical primary particles of about 10–30 nm, that then undergo surface growth (and possibly competing oxidation reactions), and agglomeration into larger fractal structures, with a typical size between 200–300 nm.[22,25–30]

From an experimental point of view, the least tractable phase of this process is the initial inception process that forms three-dimensional structures from planar PAH. The experimental difficulty in measuring this inception region has led to questions in terms of the size of PAH (generally characterized by molecular weight or number of aromatic rings) where inceptions occurs,[31–33] as well as the role of aliphatic branches, aliphatic linkages, and pentagonal rings.[34–36]

Our working hypothesis has been that inception begins with the agglomeration of pericondensed, hexagonal PAH species that are large enough that "sticking" is thermodynamically favoured at flame temperatures.[9,37,38] In an effort to provide *in situ* validation

Department of Chemistry George Washington University 800 22nd St, NW Suite 4000, Washington, DC 20052, USA. E-mail: houston@gwu.edu

† Electronic supplementary information (ESI) available: Tabulated list of the molecules studied, structural and topological descriptors, computed excitation energy of the HOMO–LUMO transition, and homo-molecular binding energies. See DOI: 10.1039/c7cp06048c

of this theory, our lab has analysed hyper-spectral extinction measurements in a variety of diffusion flames, with Tauc/Davis–Mott analysis in order to map the optical band gap (OBG) of soot as a function of flame position.[8,10,11] Similar methodologies have been used to study soot in other flame systems[39–48] as well as coal combustion.[49] Tauc/Davis–Mott analysis uses the near-edge of an absorption feature as a probe of the localized states, such that the OBG, can be calculated from eqn (1).

$$h\nu\cdot\alpha \approx (h\nu - E_g^{opt})^r \quad (1)$$

where α is the extinction coefficient, E_g^{opt} is the OBG, and r is a constant related to the quantum mechanical allowedness and directness of the optical transition.[50–53]

In order to correlate optical band gaps to molecular size, Robertson proposed the cluster model as a simple way to study the electronic structure in planar sp^2 system within a larger amorphous carbon system (sp^3 bonding), finding that the band gap was inversely proportional to the square root of the number of aromatic rings (M).[54] To expand on this work, we postulated that the electronic properties of soot are determined by the molecular structure of PAH that comprise them and that the difference between the highest occupied molecular orbital (HOMO) and lowest unoccupied molecular orbital (LUMO) is an approximation of the OBG. For our initial study relating molecular size to HOMO–LUMO gap, excited state TD-DFT computations on 4 D_{2h} molecules (pyrene, ovalene, circumpyrene, and circumovalene) were carried out using the GAMESS-US computational chemistry package. Optimized molecular geometries for the calculations were obtained from the Theoretical Spectral Database of Polycyclic Aromatic Hydrocarbons.[55] Using the functional form proposed by Robertson, the HOMO–LUMO gaps of these structures gave a linear fit, eqn (2), with the slope nearly identical to that suggested by Robertson.[10,54]

$$E_g^{opt} = \frac{5.8076}{M^{-1/2}} + 0.5413 \quad (2)$$

In all of the liquid and gas-fuelled diffusion flames studied with Tauc/Davis–Mott analysis in our work, a consistent average experimentally determined OBG of approximately 2 eV was measured, which correlates to PAH with a conjugation length of about 1 nm, based on eqn (2).[8,10,11] While a consistent OBG was determined, the specific correlation of the experimental OBG to a molecular size hinges on the assumptions that soot is comprised of highly symmetric and nearly circular PAH, and that the HOMO–LUMO gap of isolated PAH is an approximation of the aggregated PAH structures in soot. A goal of understanding these assumptions has motivated additional computational studies of the effects of both agglomeration and topology on PAH HOMO–LUMO gaps.

In a recent study the physical structure and composition of PAH stacks and clusters was correlated to their electronic properties to gain insight into the effects of intermolecular interaction on the spectral properties of nascent particulate.[16] Kohn–Sham HOMO–LUMO gaps of monomers, stacks, and clusters of six high symmetry PAH (pyrene, coronene, ovalene, circumpyrene, circumcoronene, and circumovalene) computed by DFT calculations using the NWChem platform were studied.[16] The same general trend of a decrease in HOMO–LUMO gap with an increase in monomer size was found. Additionally, homogeneous stacks and clusters had substantially lowered HOMO–LUMO gaps compared to isolated molecules with the formation of dimers and formation of clusters (two or more stacks) being the most dominant contributions. However, the agglomeration effect was found to be secondary to the molecular size of the composite PAH, such that in homogeneous clusters an asymptotic band gap limit was reached with an average decrease in band gap from monomer to cluster of about 1 eV.[16]

In this recent cluster manuscript, only PAH with relatively high symmetry (D_{2h} or D_{6h}) were studied. In the current study, we present calculations for PAH that represent a much greater diversity of topologies. In part, this work is motivated by recent advances in the asphaltene literature, specifically the work of Ruiz-Moralez *et al.*, who have explored the relationship between molecular topology and electronic structure to aid in data analysis of experimental techniques and to better understand the physical structure of asphaltenes.[3,4,56–60] Throughout these works, Ruiz-Moralez *et al.*, correlate computational studies of HOMO–LUMO gaps of PAH with fluorescence emission experimental studies to attempt to determine the size range of the base PAH unit, the number of PAH in the polyaromatic core, and the binding mechanism, a cross-linked archipelago or stacked-island architecture, of asphaltenes.[3,4,56–60]

It is the goal of this paper to take a similar approach for combustion applications: to explore the interplay between molecular and electronic structure for PAH, along with high-temperature thermodynamic stability, and the implications for their role as soot particle precursors.

Methodology

Computations

In the current study, a series of 444, PAH molecules were evaluated, 38 of the structures had aliphatic branches and 76 of the structures contained at least one, 5-membered ring. Most of these molecules are drawn from several compilations of PAH structure in the literature: PAH Databases,[55,61,62] isomer lists,[4,58,63–67] PAH types,[68,69] or combustion applications.[2,36,70–72]

The effects of molecule topology and molecular size were studied using TD-DFT computations with NWChem on George Washington University's high performance computer, Colonial One.[73] Initially molecule geometries were optimized using an MM2 molecular mechanics method. Further geometry optimization was performed using NWChem DFT computations with the 6-31G* basis set and B3LYP exchange correlation functional.[62] DFT Geometry optimizations used a root mean square gradient (RMS) threshold of 3×10^{-4} and a RMS cartesian step threshold of 1.2×10^{-3} atomic units. TD-DFT computations used the same basis set and exchange correlation function, while also excluding triplet states and using the Tamm–Dancoff approximation.[73] A TD-DFT convergence threshold of 1×10^{-4} Hartree was used.[73]

The B3LYP functional is used by Malloci *et al.* in the theoretical spectral database of PAH, where through their extensive benchmarking it has been shown to provide accurate ground-state properties and has been shown to yield accurate excited state results for the HOMO–LUMO gap.[55,62,74]

The reported TD-DFT excitation energies of the HOMO–LUMO transition will be referred to as the TD-DFT optical gap, as defined by Malloci *et al.*[62] However, for the purposes of this study this will be treated as equivalent to the HOMO–LUMO gap.

Atom-pair minimization

In 2008 our group published a paper reporting the binding energies of Stein and Fahr stabliomers.[13] (Stabliomers refers to PAH isomers for a particular carbon and hydrogen inventory that are the most thermodynamically stable.) In this work an atom-pair minimization (APM) algorithm was developed, which allowed for the optimization of geometries of PAH stacks and clusters through binding energy minimization. The APM algorithm has been used in the study of the effects of agglomeration on electronic structure[16] and is used in this work to provide some insight on the effect of topology on binding energy of PAH dimers.

Clar structures and defining topology

The HACA mechanism, which leads to PAH growth in combustion (and other) systems, is a series of hydrogen abstractions followed by successive acetylene additions. This process generally leads to PAH growth by the addition of aromatic rings to a PAH, making the number of rings in the system a convenient and common base unit for benchmarking the size of a PAH. However, a PAH with the same number of rings can be oriented in a variety of different ways and it is the configuration of the rings comprising a PAH that define its topology. To link the electronic and topological characteristics of PAH a set of topological descriptors must first be defined.

Because they fall within the more widely spaced energy σ states, transitions from populated to unpopulated levels in PAH occur within the π state manifold.[54,75] The π electrons in a conjugated system are typically delocalized leading to an enhancement in the stability, known as aromaticity, that also affects the electronic structure.[1] While the HOMO–LUMO gap of PAH decreases with an increase in molecular size, non-uniform π electron distribution across PAH introduces secondary topological effects on the band gap.[4]

The Clar model is a method of studying the aromaticity of a structure. In Clar structures, the π electrons in a polycyclic ring structure are assigned so that the maximum number of rings have 6π electrons, known as an aromatic sextet.[1] In structures comprised entirely of rings with sp^2 bonding this leads to 4 types of rings: aromatic sextets (denoted by inscribed circles), rings with one double bond (Dbl(1)), rings with two double bonds (Dbl(2)), and empty rings that have no π electrons formally associated with that ring. Aromatic sextets cannot be located in conjoined rings (rings that share a carbon–carbon bond). As long as the maximum number of aromatic sextets is realized, more than one Clar structure can contribute to the actual (average) configuration.[1,4,57,76,77] The Clar structure approach to understanding molecular structure has been validated by both atomic force microscopy and scanning tunnelling microscopy.[78]

Assigning Clar structures to molecules can aid in the understanding of their stability and their electronic structure. The kinetic and thermodynamic stability of isomers increases with an increase in number of aromatic sextets because of additional resonance energy.[1] Comparatively, aromatic ring systems with more isolated double bonds are more reactive and less stable.[63] These concepts were experimentally verified beginning in 1958, when Clar and Zanger used the Diels–Alder reaction as a measure of reactivity for a series of isomers.[76] It was found that the rings with isolated double bond character are more chemically reactive than isomers with more aromatic sextets.[76,78] Electronically, this lower reactivity is related to the wider HOMO–LUMO gap and energetic unfavorability of adding electrons to high LUMO states or removing electrons from low HOMO states.[4] These observations over a range of studies have led to the correlation of higher HOMO–LUMO gaps (within isomers) with kinetic and thermodynamic stability and lower reactivity. Thus, these larger HOMO–LUMO gaps are realized when there are more aromatic sextets in a structure.[1,4,57,63,76,78]

Fig. 1 reports the computed TD-DFT optical gaps for a series of benzenoid four-ring molecules. Tetracene is an acene (linear PAH structure) and it is only possible to draw a Clar structure with a single aromatic sextet. However, this sextet can delocalize over several rings (known as a migrating sextet). Because the aromatic sextet is shared across all the rings, the stabilization effect of the aromaticity decreases with increasing annellation. This is the reason that the thermodynamic stability of acenes decreases with size.[1,76] The nearly linear decrease in acene TD-DFT optical gap with increase in size is because the number of aromatic sextets stays constant with increases in molecular size. Pyrene, tetraphene, and chrysene are structures with the same number of aromatic sextets and similar TD-DFT optical gaps. The difference in their TD-DFT optical gaps is based on the number of Clar structures that can be drawn for a single structure because of the ability for an aromatic sextet to migrate. Pyrene has a single Clar configuration, while tetraphene and chrysene have two. Tripheylene's Clar structure is comprised

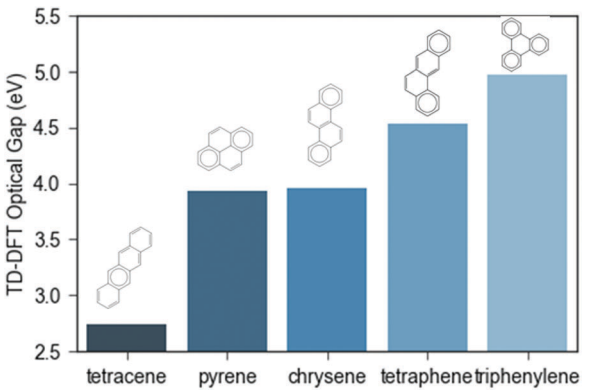

Fig. 1 Computed TD-DFT band gap (eV) for a series of benzenoid 4 ring molecules.

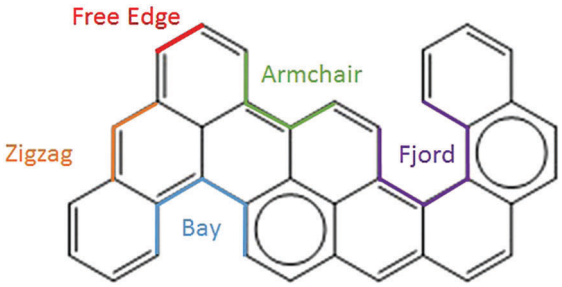

Fig. 2 PAH edge types as defined in ref. 80 and illustrative Clar structure.

entirely of aromatic sextets and empty rings, defined as a completely benzenoid system. Systems with these characteristics will be the more thermodynamically stable, less reactive, and have higher HOMO–LUMO gaps than their isomers.[1,79]

The ring types in Clar structures (aromatic sextets, empty, Dbl(1), and Dbl(2)) are useful descriptors of the topology of PAH. To further delineate topology, we identify five edge types with the naming convention of Kraft and coworkers (Fig. 2):[68,80] free edge (one edge), zigzag (two edges), armchair (three edges), bay (four edges), and fjord edge types (five edges). These edge types are related to the carbon atom types used in the intermolecular potential work by our group[13,37] and in group additivity approaches used by others to predict thermodynamic stability of PAH.[2,66,67,81] In these carbon-type approaches there are only three edge carbon types (and two additional interior carbon types). While these carbon types are able to define the carbon atoms belonging to free edge, zigzag, and armchair groups, these calculations lack enough unique carbon types to describe the carbon atoms in bay and fjord edge groups.

HOMA analysis

A variety of different algorithms and techniques have been presented to characterize the aromaticity of a molecule from its structure.[4,57] In this work, we use the harmonic oscillator model of aromaticity (HOMA) approach to aid in the identification of Clar structures.[82] This method postulates that the bond length determines the harmonic oscillator energy associated with extending or compressing a bond between that of a characteristic single (C_s) or double bond (C_d). There is an optimal bond length (R_{opt}) at an intermediate energy located in the median of these two extremes. Gas-phase electron diffraction measurements of 1,3-butadiene are used to determine the R_{opt} for a conjugated carbon–carbon system (1.388 Å, C_s −1.467 Å, C_d −1.349 Å) and the normalization parameter, α (257.7). The HOMA index can then be calculated through eqn (3) by averaging over the bond lengths of the molecule, R_i, in a system comprised of n bonds. The closer to one the HOMA index is, the more aromatic the structure or substructure.[83–86]

$$\mathrm{HOMA} = 1 - \frac{\alpha}{n}\sum_i (R_{opt} - R_i)^2 = 1 - \mathrm{EN} - \mathrm{GEO} \qquad (3)$$

The HOMA index has also been decomposed into two components, EN (eqn (4)) and GEO (eqn (5)). The EN component quantifies the elongation in the bond length leading to decrease in aromaticity by computing the normalized square of difference between the optimal bond length and average bond length. A larger EN value is indicative of lower electron density, and an empty ring in a Clar structure. The GEO component is a measure of the bond length alternation, which also decreases the aromaticity, and is related to the normalized deviation in bond length. Larger GEO values indicate localized double bond character in a Clar structure.[84,85]

$$\mathrm{EN} = \alpha(R_{opt} - R_{av})^2 \qquad (4)$$

$$\mathrm{GEO} = \frac{\alpha}{n}\sum_i (R_{av} - R_i)^2 \qquad (5)$$

In this work the HOMA index and GEO and EN components were calculated and mapped for each ring and over the entire molecule using the geometry optimized molecular coordinates. Because the HOMA index only accounts for geometric factors (bond lengths) to determine the aromatic character, results can lead to the overestimation of aromaticity in systems with equal bond lengths[4,84] and in cases of migrating sextets or geometries based on the combination of Clar structures, the HOMA values can be inconclusive or misleading.[78]

While there are limitations, the HOMA index may yet be a valuable tool in the determination of the Clar structures. For example, HOMA plots were compared to molecular electrostatic potentials calculated using DFT.[87] In the HOMA plots shown in Fig. 3, the dot in the centre of the ring indicates the HOMA index for that ring, which generally correlates with electrostatic potential for that ring in the surface plots. The HOMA plots indicate where there may be sextet migration in rings (tetracene or top of tetraphene), while also making it clear which rings have little aromatic character (centre of triphenylene and the "elbow" ring of tetraphene). In tetracene the HOMA plot shows equal HOMA values throughout all rings, where the surface plot shows higher density at the edges, an artefact of the HOMA analysis only being based on bond lengths. Thus, the HOMA index may be used to predict and differentiate between ring types that correlate with expectations for corresponding Clar structures.

Results

HOMO–LUMO gap trends

Circular catenation. In the original correlation between HOMO–LUMO gap and molecular size published by our group, only D_{2h} molecules were considered and it was found that there was a linear trend between $M^{-1/2}$ (M = number of rings) and the HOMO–LUMO gap, supporting the relationship proposed by Robertson.[88] Our hypothesis is that the rate of decrease in HOMO–LUMO gap with increases in molecule size will be similar if the topology of structures studied is similar. This hypothesis is supported by a 2002 work by Ruiz-Morales, which showed distinct power-law fits of HOMO–LUMO gap with the number of rings for linear, circular, and zigzag PAH structures.[4]

To demonstrate this effect beyond D_{2h} molecules, a series of molecules were constructed using the circular catenation method. This involves starting with a single ring and then adding rings in a

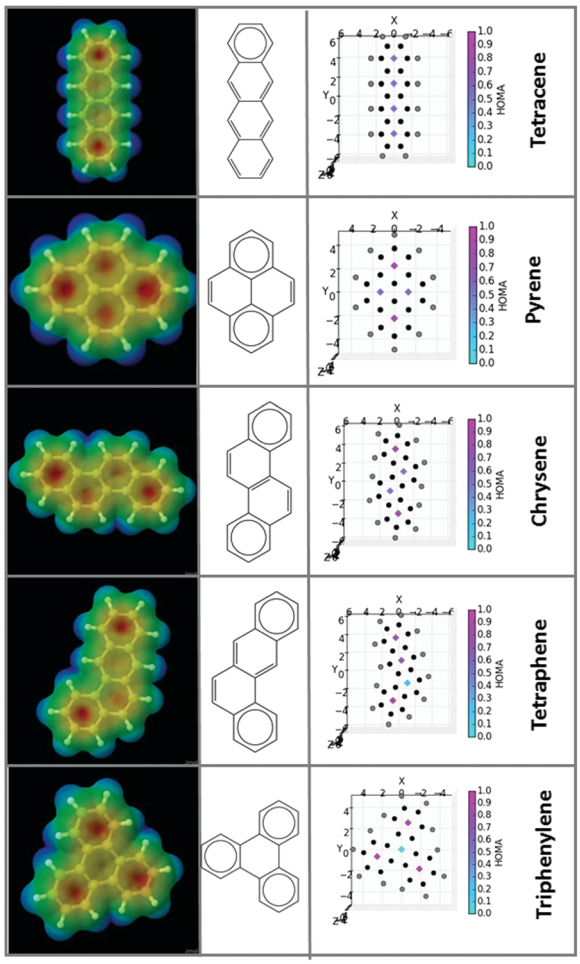

Fig. 3 Comparison of molecular electrostatic potential surface (left), Clar structure (center), and HOMA plot (right). Electrostatic potential surface (left): red depicts increased the highest electron density, where blue indicates the lowest electron density. HOMA plot (right) color bar indicates the HOMA index, where the closer the value is to 1 the higher the aromatic character in that ring.

spiral manner, with an additional requirement being that each structure had an even number of hydrogen atoms. Fig. 4 depicts the TD-DFT optical gap and average bond length as a function of number of rings for the circular catenation series. The general trend of a decrease of TD-DFT optical gap with increase in the number of rings is followed. Additionally, the average bond length elongates with an increase in molecular size. When these roughly circular structures increase in size the periphery carbons become a smaller percentage of the total carbon types. Because the edges of the molecule determine its topology of a molecule, when these edges make up less of the total number of carbons, the nearly equal bond lengths in the centre of structures lead to a decrease in the deviation of bond lengths and the average bond length approaches an asymptote equal to the monolayer bond length in graphene, 1.425 Å.[7,89]

$C_{32}H_{16}$ 9-ring isomers

As was demonstrated in the introduction of Clar structures (Fig. 1) topology can have a critical role on the determination of

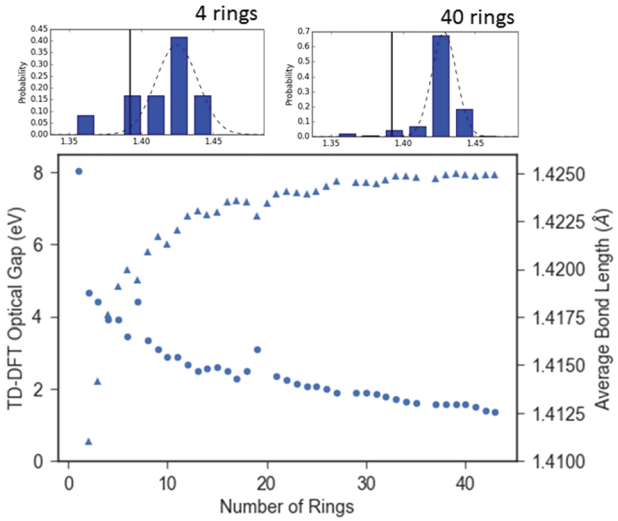

Fig. 4 TD-DFT optical gap (circles) and average bond length (triangles) as a function of number of rings for the circular catenation PAH series. Subsets: bond length histograms for 4 ring and 40 ring (black line represents the optimal bond length for a conjugated carbon–carbon bond based on HOMA analysis).

the HOMO–LUMO gaps. To better explore the nuances of this, a study of $C_{32}H_{16}$, 9-ring isomers was performed.[58] In Fig. 5, the TD-DFT optical gaps of 45 different 9 ring $C_{32}H_{16}$ isomers as a function of the number of aromatic rings are plotted. The figures in the graphs then show the structure with the largest HOMO–LUMO gap and the smallest HOMO–LUMO gap for 2, 3, 4, and 5 aromatic sextets in the molecule. These 50 isomers have an average HOMO–LUMO gap of 2.80 eV and a range of 1.92 eV. Sorting the molecules by the number of aromatic sextets still yields large band gap ranges: 2 aromatic sextets – mean 2.01 eV and range 0.16 eV, 3 aromatic sextets mean

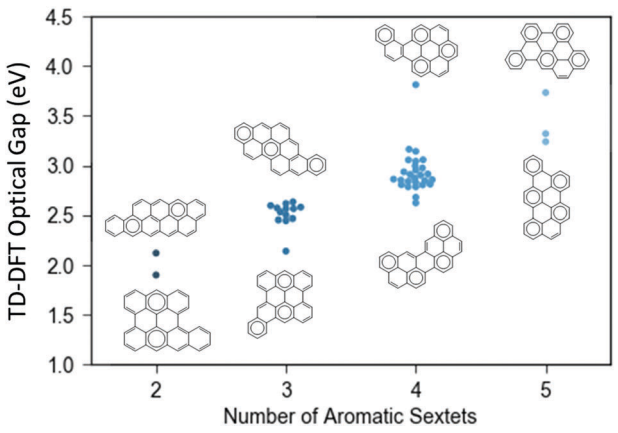

Fig. 5 Comparison of $C_{32}H_{16}$ nine ring systems with the TD-DFT optical gap (eV) as a function of number of aromatic sextets depicts the range in HOMO–LUMO gaps within structures with similar, but not identical topologies. 2 aromatic sextets – mean TD-DFT optical gap 2.01 eV with range of 0.16 eV, 3 aromatic sextets mean TD-DFT optical gap 2.51 eV with range of 0.13 eV, 4 aromatic sextets – mean TD-DFT optical gap 2.93 eV with range of 0.22 eV, and 5 aromatic sextets – mean TD-DFT optical gap 3.43 eV with range of 0.27 eV.

2.51 eV and range 0.13 eV, 4 aromatic sextets – mean 2.93 eV and range 0.22 eV, and 5 aromatic sextets – mean 3.43 eV and range 0.27 eV. Despite the large spreads in this data, the general trend is observed that within a given isomer the structure with the largest number of aromatic sextets will generally have the largest HOMO–LUMO gap (eV). Plotting the same data set against other topological parameters gives an idea about these features on the HOMO–LUMO gap. The correlation between aromatic sextets and empty rings leads to an increase in HOMO–LUMO gap with an increase in the number of empty rings. A parabolic effect is observed with the number of Dbl(1) rings with the largest HOMO–LUMO gaps being observed in structures where the number of Dbl(1) is two, but after that increasing the number of Dbl(1) bonds decreases the HOMO–LUMO gap. This contrasts with Dbl(2) rings, which always destabilize the structure. There is no distinguishable trend with HOMO–LUMO gaps and edge group type, with the exception of free edges, which show a slight increase in HOMO–LUMO gap with the increase in the number of free edge groups.

However, the presence of arm-chair structures on the periphery of a PAH tend to increase the number of aromatic sextets that can be formed compared to the zigzag edges, leading to higher HOMO–LUMO gaps.[68] Fjord (and to a lesser extent bay) structures may introduce non-planarity because of the steric interference between hydrogens. This non-planarity increases σ-bond character and subsequently can increase the HOMO–LUMO gap.[63,68,90]

Pentagonal rings

The potential for the HACA mechanism to introduce 5-membered rings at zigzag edge groups may lead to an impact of 5-membered rings on PAH stability and observed band gaps in combustion systems.[91] The literature is conflicted over whether these structures will then desorb to form PAHs comprised entirely of six-membered PAH[91] or whether these structures will persist and play an integral part in soot formation.[70]

For the most part the same general trends observed in benzenoid-only ring systems were found in structures containing five-membered rings because of the inherent non-aromaticity and low electron density in these rings. This leads to the importance of pentagonal ring location and the introduction of symmetry effects in terms of the HOMO–LUMO gap.[69] Additionally, the introduction of non-planarity from interior 5-membered rings can introduce σ-character into a system, which increases the HOMO–LUMO gap.[90]

Aliphatic branches

In addition to the presence of 5-membered rings, the presence of aliphatic branches on PAHs comprising soot is a subject of debate in the soot community.[92] These side chains may be formed through the same HACA mechanism, but without subsequent ring closure. To study the effects of aliphatic branches on electronic structure of PAH, some PAH structures cited in the soot literature were used in our computations.[2,70,71] The aliphatic branches are not part of the core aromatic structure and therefore they retain their strong, double or triple bond character compared to atoms in the rings, which may have non-integer bond orders.

There is a correlation between the observed difference in average bond length with the addition of an aliphatic branch and the change in HOMO–LUMO gap. As would be predicted, sp^3 carbons in the side chain increase the average bond length, while alkenes and alkynes tend to decrease the average bond length. Because the HOMO–LUMO gap of PAHs is dominated by the π character of these molecules, the alkane branches would have little effect on the HOMO–LUMO gap. When the average bond length decreases with the addition of an aliphatic branch, the HOMO–LUMO gap tends to also decrease, with the larger changes in bond length correlating to larger changes in HOMO–LUMO gap.[75] However, these trends change from base molecule to base molecule potentially due to further stabilizing/destabilizing effects that aren't quantified in the bond length changes. This leads to large uncertainties in the effect of adding an aliphatic branch to a molecule on the HOMO–LUMO gap.

HOMO–LUMO gap taxonomy

The complete set of molecules studied provide a database of structures that allow for searching of HOMO–LUMO gaps that match a desired optical band gap. In the five-membered ring and aliphatic branch containing structures, the HOMO–LUMO gap was found to depend on factors beyond basic topology, such as symmetry, planarity, and location, making them difficult to model without the inclusion of these factors. However, extending the topological trends observed in the circular catenation study and $C_{32}H_{16}$ 9-ring system to the larger set of benzenoid systems studied, our hypothesis was supported in that molecules with similar topological properties show similar changes in HOMO–LUMO gap with an increase in size.

We report on a taxonomy for PAH structures based on designated PAH types or relationships between different topological properties for uncategorized PAH, which then allowed for the relationship between size and HOMO–LUMO gap to be modelled past circular D_{2h} structures.[10] As expected the HOMO–LUMO gap decreases as a function of size, but the rate of that decrease is directly related to the topology of the molecules.[4] By categorizing molecules into similar topologies, plots of TD-DFT optical gap *versus* number of rings or ratio of number of aromatic rings to number of rings can be fit with simple functional forms.

To develop the model, PAH were first split into similar PAH categories before being fit to power functions. The first PAH types were ones that already belonged to a defined PAH class: all benzenoid, acenes, perylenes, rylenes, coronene series, and circular D_{2h} series (this was not an exclusive label and circular D_{2h} molecules were used in other fits). The coronene series is comprised of coronene, circumcoronene, and circumcircumcoronene (all sharing D_{6h} symmetry). The circular D_{2h} series is comprised of naphthalene, pyrene, ovalene, circumpyrene, circumovalene, and circumcircumpyrene.

All category definitions (other than circular D_{2h} and coronene categories) are defined according to the flow chart shown in Fig. 6 based on existing PAH class, the presence of isolated double

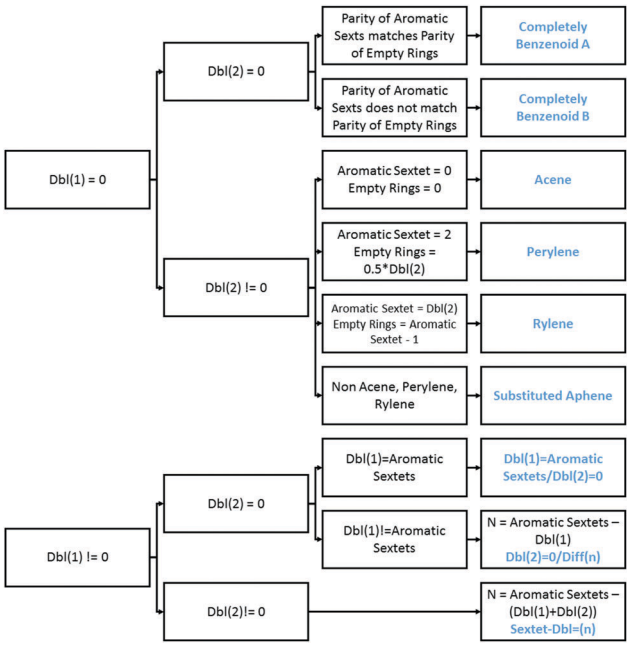

Fig. 6 Flow chart illustrating classification system for PAH morphology.

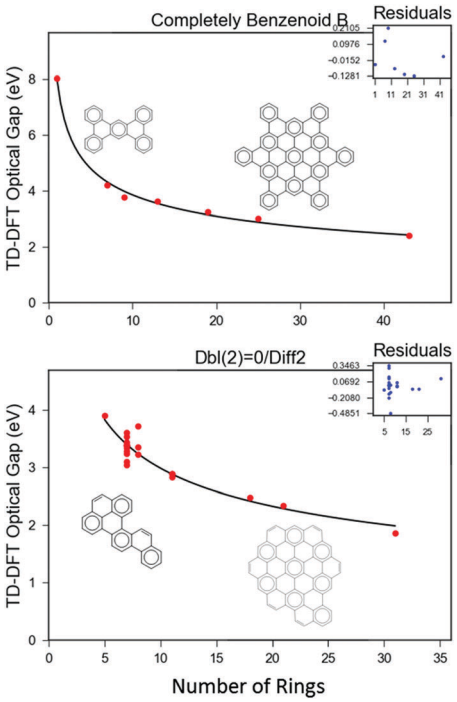

Fig. 7 HOMO–LUMO gap fit results from completely benzenoid B and Dbl(2) = 0/Diff2 PAH.

bonds, and the relationship between the number of aromatic sextets and number of isolated double bonds. The literature suggests that the ratio of double bonds to number of aromatic sextets is a factor that impacts the HOMO–LUMO gap the greatest after the total number of rings and the number of aromatic sextets.[4,60,63] However, in developing this model it has been found that the difference between the number of aromatic sextets and the number of rings with isolated double bonds in a structure better categorize PAH when grouped within the larger categories relating to whether the number of isolated double bond is equal to zero.

PAH categories were then modelled with power fits with TD-DFT optical gap as a function of the number of rings. The exception to this is the substituted aphenes, which were fit as a function of the ratio of aromatic rings to the number of rings in the structure. Fig. 7 presents examples of the fits for the structures with no Dbl(2) rings and where there are two more aromatic sextet then Dbl(1); and completely benzenoid structure with mismatched parity between empty rings and aromatic sextets.

If there were not at least three structures in a category the data was not fit. Additionally, the residuals and R^2 value for each fit is saved, so it can act as a threshold to identify poor fits. Table 1 shows results with an R^2 threshold of at least 0.7. Ruiz reported a power fit for linear PAH, which agrees within an average of 20% for the acene model reported here, when comparing within the overlapping PAH size range.[4]

For a given molecular formula and number of rings, there are a large number of PAH isomers that have distinctly different optical gaps based on their topology. The reported PAH taxonomy classifies PAH into categories so within each group the optical gap is able to be modelled as a function of molecular size. This allows researchers looking to compare experiment optical band gap and absorption measurements with theory to quickly determine the size of relevant structures across a broad variety of topologies. For example, single PAH structures as small as five rings in the acene topology group or as large as seventy rings in the fully benzenoid topology group each have band gaps near 2 eV.

While the ability to determine the size of a variety of PAH with a certain band gap greatly extends the ability to correlate experimentally determined band gaps with molecular sizes, the PAH taxonomy is limited by its inability to separate structures that have the same number of Clar ring types and by only including purely hexagon-comprised structures. Both limitations suggest that the quantification and addition of higher level topological considerations such as symmetry, planarity, and location might remove these limitations. Additionally, having a HOMO–LUMO gap that matches the experimentally determined OBG is only one criteria in deciding if a PAH may play a role in the particle inception process. Other critical parameters include PAH binding energy and thermodynamic stability.

Binding energy

Over the last decade our lab has been conducting a range of studies attempting to determine the size of PAH involved in the particle inception region of the soot formation process.[8–11] In an inception process that is based on non-bonded interactions, the binding energy (BE) of an incipient dimer needs to be strong enough so the dimer can survive at flame temperatures.

A 2008 publication from our group evaluated binding energies in dimers of Stein and Fahr stabliomers to correlate size of PAH and the strength of non-bonded interactions in

Table 1 HOMO–LUMO Gap as a function of size for each PAH taxonomy class with more than 3 structures and an R^2 greater than 0.7 (TD-DFT optical gap (eV) = $a \times$ (fit type)^b)

PAH morphology type	Fit type	Count	a	b	Model min fit value	Model max fit value	R^2
Completely benzenoid A	Number rings	10	7.071	−0.298	4	34	0.84
Completely benzenoid B	Number rings	7	7.996	−0.317	1	43	1.00
Circular D_{2h}	Number rings	6	5.978	−0.327	2	30	0.99
Coronene	Number rings	3	9.153	−0.372	7	37	1.00
Acene	Number rings	8	8.913	−0.891	2	9	0.99
Perylene	Number rings	3	12.541	−0.858	5	11	1.00
Rylene	Number rings	4	7.469	−0.528	8	17	1.00
Sub aphene	Aromatic sextets /number rings	26	5.886	0.766	0.2	0.6	0.78
Dbl(1) = aromatic sextets/Dbl(2) = 0	Number rings	19	6.222	−0.352	4	33	0.96
Dbl(2) = 0/Diff-1	Number rings	6	6.223	−0.348	7	27	0.93
Dbl(2) = 0/Diff1	Number rings	33	6.864	−0.368	3	61	0.88
Dbl(2) = 0/Diff2	Number rings	21	6.846	−0.360	5	31	0.87
Sextet-Dbl = −1	Number rings	41	6.486	−0.409	5	43	0.82
Sextet-Dbl = 1	Number rings	26	6.951	−0.387	6	40	0.76
Sextet-Dbl = 2	Number rings	13	6.049	−0.313	8	18	0.75
Sextet-Dbl = 0	Number rings	59	7.901	−0.466	4	41	0.74

PAH agglomeration. A critical finding was that the binding energies of homomolecular dimers rise rapidly with molecular size before asymptotically reaching the exfoliation energy for graphite of 5 kJ mol^{-1} carbon atom^{-1}.[13] An empirical fit was used to model this behaviour and is shown as a dashed line in Fig. 8. Including the binding energies of homomolecular dimers of benzenoid structures studied in the current study, shows that the varying topologies beyond approximately circular stabliomers has a substantial effect on the binding energy per carbon atom in the monomer. Because the APM algorithm used to calculate the binding energy is based on carbon types, structures with bay and fjord functionalities are not included. (This also excludes 5-membered rings and aliphatic linkage containing structures from this study.)

Violi *et al.* used an atomistic model to calculate the free-energy profiles of a variety of PAH dimers and trimers to determine the stability of agglomerates. A conclusion derived from their work was that mass alone was not completely responsible for differences in PAH dimer stability, but that the symmetry of these structures also played a part, with low symmetry structures dimerizing more than higher symmetry structures.[92] While the BE is only a contributing factor to the dimerization stability in PAH, the potential for symmetry effects on BE proved a logical option for the deviation in BE over structures with the same size, but varying topologies. The symmetry group of PAH structures was determined and it was found that there was not a significant correlation between symmetry group and binding energy because a single symmetry group can span a range of different structure types. In the D_{2h} symmetry group, the entire series of acenes, rylenes, perylenes, and circular D_{2h} structures (along with assorted miscellaneous structures) are included marking a progression from linear to circular structures.

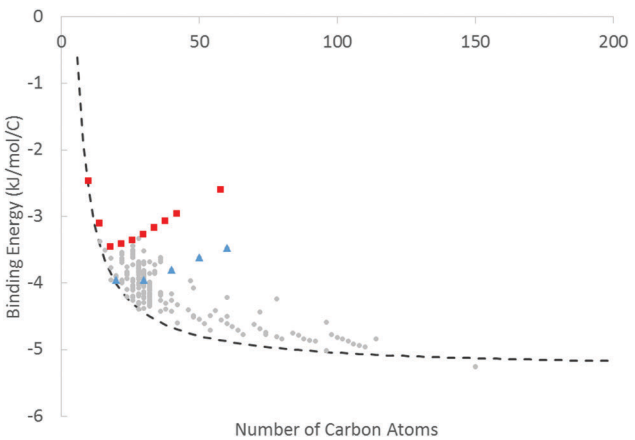

Fig. 8 Binding energy as a function of number of carbon atoms in the monomer for the complete set of benzenoid molecules studied. The dashed line depicts the empirical binding energy relationship for Stein and Fahr stabliomers found in a previous work. The red squares show the binding energy for acenes and the blue triangles show the binding energy for rylenes.

The dashed line shown in Fig. 8 defines the lower limit of binding energy behaviour. Circular D_{2h} and coronene structures, that were also studied in the previously published BE work,[13] follow the modelled behaviour closely with deviations below 5%. The plane-parallel, displaced geometry that is the favoured conformation of PAH dimers[13] will provide more overlap and potential for intermolecular interactions if the structures are more circular. Acenes (shown in red squares in Fig. 8) depict this behaviour with an initial decrease in BE and then a subsequent increase in BE per carbon atom. In these linear structures the centre of both molecules in the dimer overlap in the APM optimized geometry, but as continued annellation occurs the overlap, and resulting magnitude of the BE, does not increase with the increase in number of carbon atoms. This same trend is exhibited in the rylene series (blue triangles in Fig. 8).

The circular catenation data set provides a demonstrative case study for the link between binding energy and circularity in PAH. The study is designed so the structures are mostly circular with highly symmetric-circular molecules being formed at intervals as rings are added. In addition to the overall decrease in binding energy per carbon with an increase in molecule size, this data set shows a sawtooth pattern with local minima occurring at the high symmetry structures. Fig. 9 focuses on

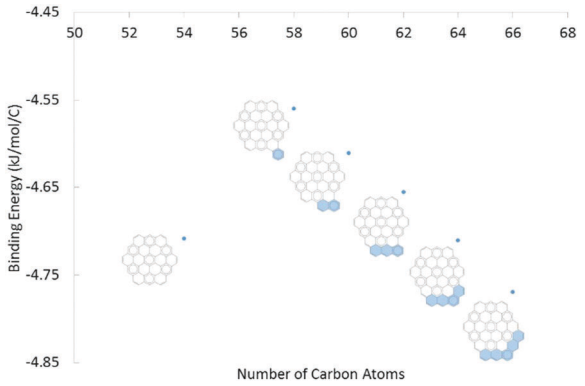

Fig. 9 Binding energy per carbon atom as a function of number of carbon atoms for PAH in the circular catenation series with 19–24 rings. Rings with blue shading represent the rings added in the series progression compared to the circumcoronene (19 rings).

the circular catenation series between 19 and 24 rings, which correlates to the transition between circumcoronene and circumovalene. This figure shows that the local BE minima in this series correlates to the most circular structures. The BE then increases sharply with the addition of an additional ring to the periphery with a decrease in BE as rings approaching another highly circular structure.

Ruiz *et al.* reported a definition for PAH percent circularity,[4] based on the number of rings in a system, where the circularity is bound by acenes at 0% circularity and pericondensed structures with 100% circularity.[4] This metric was used to quantify the trend that more circular structures tended to have a lower BE compared to linear structures. There is a consistent decrease in the BE with an increase in the percent circularity. Within structures with the same number of carbon atoms and number of rings, topological parameters have additional effects on the binding energy. Because carbon atom types, which are synonymous with the edge group types defined in Fig. 2, are used to calculate BE; these edge groups inherently determine the relationship between BE and topological properties. Increases in the number of armchair and free edge groups cause a decrease in the BE, while an increase in the number of zigzag sites causes an increase in the BE. The BE decreases with an increase in the number of aromatic sextets, and there is no correlation between Dbl(1) and Dbl(2) and BE.

The increase in the strength of the non-bonded interactions with an increase in the circularity is related to the overlap between the monomeric components of the dimer in preferred plane-parallel displaced geometry of PAH dimers. However, just as in the HOMO–LUMO gap studies, topological effects are secondary considerations to overall size of the PAH in regards to the binding energy per carbon. The combination of these conclusions, leads to the conclusion that a less circular PAH needs to be larger to have the same binding energy per carbon as a more circular structure.

Linking HOMO–LUMO gap and high temperature stability

The studies presented in this paper focused on understanding the effects of PAH topology on both electronic structure and binding energy with a goal of understanding the types of PAH that might be involved in the particle inception process during soot formation. An important consideration in this application is the determination of PAH structures that are thermodynamically stable at flame temperatures.

As noted above, Stein and Fahr studied the thermodynamic stability of hydrocarbons at elevated temperatures.[2] At temperatures above 1500 K, they hypothesize that thermodynamic stability dictates species formation.[2] The stabilities of $C_{2n}H_{2m}$ structures were determined by their theoretical equilibrium concentrations in the reaction of acetylene to form the PAH molecule and hydrogen. The thermodynamic properties of a PAH isomer were estimated as the sum of the comprising structural groups, known as the group additivity approach. The isomer that was deemed to be the most stable at 1500 K based on rotational symmetry, steric effects, group additivity, and polyaromatic cluster stability is listed in the Stein and Fahr stabliomer grid.[2]

Alberty *et al.* continued this work in a series of papers entitled the standard chemical thermodynamic properties of polycyclic hydrocarbons and their isomers.[66,67,81] While Stein and Fahr included structures with aliphatic side chains and five-membered rings, Alberty *et al.* focused on structures containing only six-membered rings. In addition, Alberty *et al.* include tables enumerating changes in isomer fraction (based on thermodynamic stability) as a function of temperature. In the group additivity approach, carbon types A–E are used to describe the molecular structure. This means that the stability is related to the carbon type (and therefore edge-group types) and if structures share the same edge-group statistics then the reported thermodynamic properties would be the same.[93] The complete series of Stein and Fahr stabliomers and structures studied in the work by Alberty *et al.* were studied in the current work.

At room temperature, the PAH with the highest HOMO–LUMO gap could be hypothesized to have the most stable structure.[94] However, an important conclusion of the work of Stein and Fahr was that room temperature thermodynamic stability intuition can fail at high temperatures.[2] In the structures studied in this work (including a temperature uncertainty equal to k_BT at 1500 K and not including isomers where only a single molecule was studied) there was a 62.5% agreement between the isomer with the largest band gap and the Stein and Fahr stabliomer. For example, Fig. 10 reports the isomer fraction as a function of temperature for $C_{20}H_{12}$ benzenoid-only isomers. Benzo[*e*]pyrene has the highest HOMO–LUMO gap, is the largest isomer fraction at room temperature, and the Stein and Fahr stabliomer. Benzo[*e*]pyrene and perylene show decreases in isomer fraction with increase in temperature, but the benzo[*pqr*]tetraphene isomer fraction increases with temperature. While benzo[*e*]pyrene is the most stable isomer (as determined by Stein and Fahr), all three benzenoid isomers have a substantial isomer fraction at flame temperatures. Similar trends were observed for the full range of structures, where there was overlap between these two works, indicating that more than just the Stein and Fahr stabliomer should be considered as an isomer that is stable at flame temperatures.

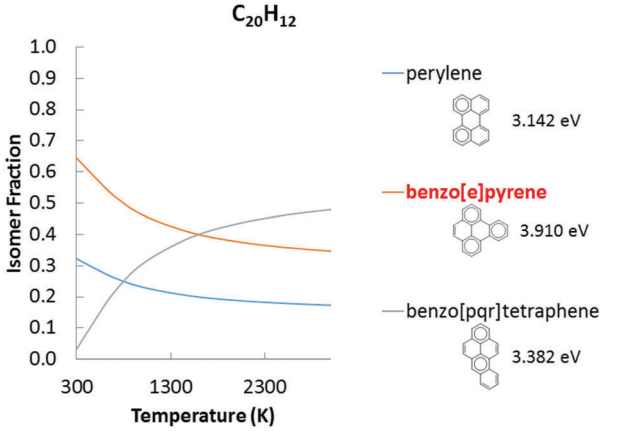

Fig. 10 Plot of isomer fraction as a function of temperature for $C_{20}H_{12}$ isomers.[67] Benzo[e]pyrene has the highest HOMO–LUMO gap, is the largest isomer fraction at room temperature, and the Stein and Fahr stabliomer. Benzo[e]pyrene and perylene show decreases in isomer fraction with increase in temperature, but benzo[*pqr*]tetraphene isomer fraction increases with temperature. However, all three species show substantial isomer fractions at flame temperatures.

The combination of the Stein and Fahr stabliomer grid[2] along with isomeric study of high temperature stability of Alberty *et al.*[66,67,81] provide a subset of structures that are known to be stable at flame temperatures. This allows us to limit the PAH structures that have HOMO–LUMO gaps that correlate to the experimentally determined optical band gap even further to those that have also been shown to be stable or have a substantial isomer fraction at flame temperatures.

Conclusions

Because of the difficulty in experimentally probing the particle inception region in flames, the size and type of molecules that play a role in this pivotal transition from 2- to 3-dimensional growth remain in question. Our lab has spent much of the last decade adding experimental evidence to support our hypothesis that particle inception occurs with the dimerization of modestly size PAH through non-bonded interactions. The most recent experiments involve analysing hyper-spectral extinction measurements with Tauc/Davis–Mott analysis to map the optical band gap as a function of flame position.[8,11,95] By computing the electronic structure of known PAH, a correlation can be made between the HOMO–LUMO gap of computed molecules and the experimentally determined optical band gap.

The work presented here explores the effects that topology of PAH has on its electronic structure as computed by NWChem TD-DFT calculations. Clar structures provide an avenue to link the physical structure and the aromaticity of the molecule. In addition to the size of the PAH, the number of aromatic sextets and the difference between the number of aromatic sextets and the number of double bonds had a large impact on the size of the HOMO–LUMO gap. The study of Clar structures led to the conclusion that all structures' band gaps decrease as a function of size, but the rate of that decrease is directly related to the topology of the molecules. By categorizing PAH into categories with similar properties, a model was developed relating the HOMO–LUMO gap to the inventory of electronic sub-features. This model allows researchers a convenient tool to determine PAH of interest across a variety of topologies. While the model currently only applies to benzenoid structures, a manual search of studied PAH with 5-membered rings can be used to find structures with similar HOMO–LUMO gaps.

The study also evaluated the binding energy for homomolecular dimers for this set of molecules with varying topologies. As is the case for HOMO–LUMO gaps, the binding energy per carbon atom decreases with an increase in molecular size and topology plays a secondary role. It was found that the circularity of the PAH structure played an important role in maximizing the magnitude of the binding energy per carbon by maximizing overlap between the monomers in the dimer.

Applying the results from these studies to combustion applications limits the range of PAH that will likely participate in particle inception. The model of HOMO–LUMO gap as a function of PAH size for a variety of PAH topology groupings can be used to find the size of the PAH in each group correlating to experimentally determined optical bands gaps. Further, the likelihood of playing a role in particle inception would then depend on circularity (and its role in binding energy of agglomerates) and monomer thermodynamic stability at flame temperatures.[2,66,67,81] These computational studies of PAH combine electronic, topological, and thermodynamic considerations to provide a robust basis of comparison to experimental measurements of carbonaceous particulates in combustion systems.

Conflicts of interest

There are no conflicts to declare.

Acknowledgements

This material is based upon work supported by the U.S. National Science Foundation under grant numbers, CBET-1142284, CBET-1706757 with Arvind Atreya, Ruey-Hung Chen, and Song-Charng Kong serving as technical monitors. This work was done on the GWU Colonial One High Performance Computing cluster with the help of Dr Glen MacLachlan. We would also like to acknowledge the help of Jennifer Giaccai in job submission management on Colonial One.

Notes and references

1 E. Clar and R. Schoental, *Polycyclic hydrocarbons*, Springer, 1964.
2 S. E. Stein and A. Fahr, *J. Phys. Chem.*, 1985, **89**, 3714–3725.
3 Y. Ruiz-Morales and O. C. Mullins, *Energy Fuels*, 2007, **21**, 256–265.
4 Y. Ruiz-Morales, *J. Phys. Chem. A*, 2002, **106**, 11283–11308.
5 X. Tan, *Spectrochim. Acta, Part A*, 2009, **71**, 2005–2011.

6 M. Frenklach, C. Carmer and E. Feigelson, *Nature*, 1979, **339**, 196–198.
7 W. Hu, L. Lin, C. Yang and J. Yang, *J. Chem. Phys.*, 2014, **141**, 214704.
8 E. M. Adkins and J. H. Miller, *Phys. Chem. Chem. Phys.*, 2015, **17**, 2686–2695.
9 J. D. Herdman, B. C. Connelly, M. D. Smooke, M. B. Long and J. H. Miller, *Carbon*, 2011, **49**, 5298–5311.
10 J. H. Miller, J. D. Herdman, C. D. O. Green and E. M. Webster, *Proc. Combust. Inst.*, 2012, **34**, 3669–3675.
11 M. L. Botero, E. M. Adkins, S. González-Calera, H. Miller and M. Kraft, *Combust. Flame*, 2016, **164**, 250–258.
12 J. H. Miller, *Proc. Combust. Inst.*, 2005, **30**, 1381–1388.
13 J. D. Herdman and J. H. Miller, *J. Phys. Chem. A*, 2008, **112**, 6249–6256.
14 M. Puccio, PhD thesis, George Washington University, 2009.
15 M. A. Puccio and J. H. Miller, *Anal. Chem.*, 2010, **82**, 5160–5168.
16 E. M. Adkins, J. A. Giaccai and J. H. Miller, *Proc. Combust. Inst.*, 2016, **36**, 957–964.
17 M. Frenklach and L. B. Ebert, *J. Phys. Chem.*, 1988, **92**, 561–563.
18 H. Wang and M. Frenklach, *Presented in part at the Fall Technical Meeting of the Eastern States Section of the Combustion Institute*, Albany, New York, 1989.
19 M. Frenklach and H. Wang, *Proc. Combust. Inst.*, 1990, **23**, 1559–1566.
20 H. Wang and M. Frenklach, *J. Phys. Chem.*, 1993, **97**, 3867–3874.
21 H. Wang and M. Frenklach, *Combust. Flame*, 1997, **110**, 173–221.
22 M. Frenklach, *Phys. Chem. Chem. Phys.*, 2002, **4**, 2028–2037.
23 N. Moriarty, X. Krokidis, W. Lester Jr and M. Frenklache, Presented in part at the Abstracts of Papers of the American Chemical Society, 2002.
24 M. Frenklach and H. Wang, *Symp. (Int.) Combust., [Proc.]*, 1991, **23**, 1559–1566.
25 T. C. Bond, S. J. Doherty, D. W. Fahey, P. M. Forster, T. Berntsen, B. J. DeAngelo, M. G. Flanner, S. Ghan, B. Kärcher, D. Koch, S. Kinne, Y. Kondo, P. K. Quinn, M. C. Sarofim, M. G. Schultz, M. Schulz, C. Venkataraman, H. Zhang, S. Zhang, N. Bellouin, S. K. Guttikunda, P. K. Hopke, M. Z. Jacobson, J. W. Kaiser, Z. Klimont, U. Lohmann, J. P. Schwarz, D. Shindell, T. Storelvmo, S. G. Warren and C. S. Zender, *J. Geophys. Res.*, 2013, **118**, 5380–5552.
26 H. Moosmüller, R. Chakrabarty and W. Arnott, *J. Quant. Spectrosc. Radiat. Transfer*, 2009, **110**, 844–878.
27 P. Buseck, K. Adachi, A. Gelencsér, É. Tompa and M. Pósfai, *Atmospheric Chem. Phys.*, 2012, **12**, 24821–24846.
28 M. Andreae and A. Gelencsér, *Atmospheric Chem. Phys.*, 2006, **6**, 3131–3148.
29 D. Lack, H. Moosmüller, G. McMeeking, R. Chakrabarty and D. Baumgardner, *Anal. Bioanal. Chem.*, 2014, **406**, 99–122.
30 H. Richter and J. Howard, *Prog. Energy Combust. Sci.*, 2000, **26**, 565–608.
31 C. A. Schuetz and M. Frenklach, *Proc. Combust. Inst.*, 2002, **29**, 2307–2314.
32 H. Wang, *Proc. Combust. Inst.*, 2011, **33**, 41–67.
33 D. Chen, T. S. Totton, J. W. J. Akroyd, S. Mosbach and M. Kraft, *Carbon*, 2014, **67**, 79–91.
34 S.-H. Chung and A. Violi, *Proc. Combust. Inst.*, 2011, **33**, 693–700.
35 S. H. Chung and A. Violi, *J. Chem. Phys.*, 2010, **132**, 174502.
36 J. S. Lowe, J. Y. Lai, P. Elvati and A. Violi, *Proc. Combust. Inst.*, 2015, **35**, 1827–1832.
37 J. H. Miller, W. G. Mallard and K. C. Smyth, *J. Phys. Chem.*, 1984, **88**, 4963–4970.
38 J. H. Miller, *Proc. Combust. Inst.*, 1990, **23**, 91–95.
39 P. Minutolo, G. Gambi and A. D'Alessio, *Proc. Combust. Inst.*, 1996, **26**, 951–957.
40 A. D'Alessio, A. D'Anna, G. Gambi and P. Minutolo, *J. Aerosol Sci.*, 1998, **29**, 397–409.
41 A. D'alessio, G. Gambi, P. Minutolo, S. Russo and A. D'Anna, *Symp. (Int.) Combust., [Proc.]*, 1994, **25**, 645–651.
42 G. Basile, A. Rolando, A. D'Alessio, A. D'Anna and P. Minutolo, *Proc. Combust. Inst.*, 2002, **29**, 2391–2397.
43 C. Allouis, A. D'Alessio, F. Beretta and A. Borghese, *Proc. Combust. Inst.*, 2000, **28**, 311–317.
44 A. Ciajolo, B. Apicella, R. Barbella and A. Tregrossi, *Combust. Sci. Technol.*, 2000, **153**, 19–32.
45 B. Apicella, M. Alfe, R. Barbella, A. Tregrossi and A. Ciajolo, *Carbon*, 2004, **42**, 1583–1589.
46 C. Russo, M. Alfè, J.-N. Rouzaud, F. Stanzione, A. Tregrossi and A. Ciajolo, *Proc. Combust. Inst.*, 2013, **34**, 1885–1892.
47 C. Russo, F. Stanzione, A. Ciajolo and A. Tregrossi, *Proc. Combust. Inst.*, 2013, **34**, 3661–3668.
48 C. Russo, F. Stanzione, M. Alfè, A. Ciajolo and A. Tregrossi, *Combust. Sci. Technol.*, 2012, **184**, 1219–1231.
49 T. C. Bond, *Geophys. Res. Lett.*, 2001, **28**, 4075–4078.
50 J. Tauc, R. Grigorovici and A. Vancu, *Phys. Status Solidi B*, 1966, **15**, 627–637.
51 D. L. Wood and J. Tauc, *Phys. Rev. B: Solid State*, 1972, **3**(5), 3144–3151.
52 E. Davis and N. Mott, *Philos. Mag.*, 1970, **22**, 0903–0922.
53 E. A. Davis and N. F. Mott, *Electronic Processes in Non-Crystalline Materials*, 2012, pp. 272–301.
54 J. Robertson, *Mater. Sci. Eng., R*, 2002, **37**, 129–281.
55 G. Malloci, Theoretical spectral database of polycyclic aromatic hydrocarbons, http://astrochemistry.ca.astro.it/database/pahs.html, accessed January 3, 2012, 2011.
56 J. P. Mathews, V. Fernandez-Also, A. D. Jones and H. H. Schobert, *Fuel*, 2010, **89**, 1461–1469.
57 Y. Ruiz-Morales, *J. Phys. Chem. A*, 2004, **108**, 10873–10896.
58 J. O. Oña-Ruales and Y. Ruiz-Morales, *J. Phys. Chem. A*, 2014, **118**, 5212–5227.
59 Y. Ruiz-Morales and O. C. Mullins, *Energy Fuels*, 2009, **23**, 1169–1177.
60 H. Groenzin and O. C. Mullins, *J. Phys. Chem. A*, 1999, **103**, 11237–11245.
61 C. Boersma, C. Bauschlicher Jr, A. Ricca, A. Mattioda, J. Cami, E. Peeters, F. S. de Armas, G. P. Saborido,

D. Hudgins and L. Allamandola, *Astrophys. J., Suppl. Ser.*, 2014, **211**, 8.
62 G. Malloci, G. Cappellini, G. Mulas and A. Mattoni, *Chem. Phys.*, 2011, **384**, 19–27.
63 F. Alvarez-Ramírez and Y. Ruiz-Morales, *Energy Fuels*, 2013, **27**, 1791–1808.
64 I. Gutman and Y. Ruiz-Morales, *Polycyclic Aromat. Compd.*, 2007, **27**, 41–49.
65 J. O. Oña-Ruales and Y. Ruiz-Morales, *J. Phys. Chem. A*, 2014, **118**, 12262–12273.
66 R. A. Alberty and A. K. Reif, *J. Phys. Chem. Ref. Data*, 1988, **17**, 241–253.
67 R. A. Alberty, M. B. Chung and A. K. Reif, *J. Phys. Chem. Ref. Data*, 1989, **18**, 77–109.
68 R. Rieger and K. Müllen, *J. Phys. Org. Chem.*, 2010, **23**, 315–325.
69 Y. Ruiz-Morales, *Can. J. Chem.*, 2009, **87**, 1280–1295.
70 K. O. Johansson, J. Y. W. Lai, S. A. Skeen, D. M. Popolan-Vaida, K. R. Wilson, N. Hansen, A. Violi and H. A. Michelsen, *Proc. Combust. Inst.*, 2015, **35**, 1819–1826.
71 J. Y. W. Lai, P. Elvati and A. Violi, *Phys. Chem. Chem. Phys.*, 2014, **16**, 7969–7979.
72 S. E. Stein and R. Brown, *J. Am. Chem. Soc.*, 1987, **109**, 3721–3729.
73 M. Valiev, E. J. Bylaska, N. Govind, K. Kowalski, T. P. Straatsma, H. J. Van Dam, D. Wang, J. Nieplocha, E. Apra and T. L. Windus, *Comput. Phys. Commun.*, 2010, **181**, 1477–1489.
74 G. Malloci, C. Joblin and G. Mulas, *Chem. Phys.*, 2007, **332**, 353–359.
75 J. B. Birks, *Photophysics of Aromatic Molecules*, 1970.
76 A. T. Balaban, *Polycyclic Aromat. Compd.*, 2004, **24**, 83–89.
77 A. T. Balaban, *Phys. Chem. Chem. Phys.*, 2011, **13**, 20649–20658.
78 M. Sola, *Front. Chem.*, 2013, **13**, 1–8.
79 M. Mueller, C. Kübel and K. Müllen, *Chem. – Eur. J.*, 1998, **4**, 2099–2109.
80 D. Chen, Z. Zainuddin, E. Yapp, J. Akroyd, S. Mosbach and M. Kraft, *Proc. Combust. Inst.*, 2013, **34**, 1827–1835.
81 R. A. Alberty, M. B. Chung and A. K. Reif, *J. Phys. Chem. Ref. Data*, 1990, **19**, 349–370.
82 F. Feixas, E. Matito, J. Poater and M. Solà, *J. Comput. Chem.*, 2008, **29**, 1543–1554.
83 J. Kruszewski and T. Krygowski, *Tetrahedron Lett.*, 1972, **13**, 3839–3842.
84 T. M. Krygowski and M. K. Cyranski, *Chem. Rev.*, 2001, **101**, 1385–1420.
85 T. M. Krygowski, H. Szatylowicz, O. A. Stasyuk, J. Dominikowska and M. Palusiak, *Chem. Rev.*, 2014, **114**, 6383–6422.
86 T. M. Krygowski, *J. Chem. Inf. Comput. Sci.*, 1993, **33**, 70–78.
87 J. Jmol, Jmol web page, http://www, jmol. org/, last accessed, 2013, vol. 15.
88 J. Robertson and E. P. O'Reilly, *Phys. Rev. B: Condens. Matter Mater. Phys.*, 1987, **35**, 2946–2957.
89 C. Feng, C. Lin, W. Fan, R. Zhang and M. A. Van Hove, *J. Chem. Phys.*, 2009, **131**, 194702.
90 C. Jäger, H. Mutschke, T. Henning, F. Huisken, C. Jäger, H. Mutschke, T. Henning and F. Huisken, *EAS Publ. Ser.*, 2011, **46**, 293–304.
91 R. Whitesides and M. Frenklach, *J. Phys. Chem. A*, 2009, **114**, 689–703.
92 P. Elvati and A. Violi, *Proc. Combust. Inst.*, 2013, **34**, 1837–1843.
93 S. Stein, D. Golden and S. W. Benson, *J. Phys. Chem.*, 1977, **81**, 314–317.
94 E. Clar, *The aromatic sextet*, John Wiley, 1972.
95 J. H. Miller, J. D. Herdman, C. D. O. Green and E. M. Webster, *Proc. Combust. Inst.*, 2013, **34**, 3669–3675.